Title
Near-resonant four-wave mixing of attosecond extreme-ultraviolet pulses with near-infrared pulses in neon: Detection of electronic coherences

Journal
Physical Review A, 94(2)

ISSN
2469-9926

Authors
Cao, W
Warrick, ER
Fidler, A
et al.

Publication Date
2016-08-08

DOI
10.1103/PhysRevA.94.021802

Peer reviewed

PHYSICAL REVIEW A **94**, 021802(R) (2016)

Near-resonant four-wave mixing of attosecond extreme-ultraviolet pulses with near-infrared pulses in neon: Detection of electronic coherences

Wei Cao,[1,2,3] Erika R. Warrick,[1,2] Ashley Fidler,[1,2] Stephen R. Leone,[1,2,3] and Daniel M. Neumark[1,2]
[1]*Chemical Sciences Division, Lawrence Berkeley National Laboratory, Berkeley, California 94720, USA*
[2]*Department of Chemistry, University of California, Berkeley, California 94720, USA*
[3]*Department of Physics, University of California, Berkeley, California 94720, USA*
(Received 27 February 2016; revised manuscript received 10 June 2016; published 8 August 2016)

Coherent narrow-band extreme-ultraviolet (EUV) light is generated by a near-resonant four-wave mixing (FWM) process between attosecond pulse trains and near-infrared pulses in neon gas. The near-resonant FWM process involves one vacuum-ultraviolet (VUV) photon and two near-infrared (NIR) photons and produces new higher-energy frequency components corresponding to the ns/nd to ground-state ($2s^2 2p^6$) transitions in the neon atom. The EUV emission exhibits small angular divergence (2 mrad) and monotonically increasing intensity over a pressure range of 0.5–16 Torr, suggesting phase matching in the production of the narrow-bandwidth coherent EUV light. In addition, time-resolved scans of the NIR nonlinear mixing process reveal the detection of a persistent, ultrafast bound electronic wave packet based on a coherent superposition initiated by the VUV pulse in the neon atoms. This FWM process using attosecond pulses offers a means for both efficient narrow-band EUV source generation and time-resolved investigations of ultrafast dynamics.

DOI: 10.1103/PhysRevA.94.021802

I. INTRODUCTION

When matter is exposed to a strong optical electric field, electrons are overdriven to produce a polarizability that is not linear with the intensity of the incident electric field. This nonlinear response is the essence of all nonlinear spectroscopies [1,2]. It is the basis for developing new frequency light sources through nonlinear optical methods including frequency doubling and tripling, four-wave mixing (FWM), and high-order harmonic generation [3–10]. The nonlinear response also underlies time-resolved studies of ultrafast dynamics in atoms [11], molecules [12–14], and solids [15,16]. Ultrafast nonlinear spectroscopy such as coherent Raman scattering, time-resolved FWM, and multidimensional spectroscopy relies on intense coherent light sources, which has developed dramatically in the optical and infrared regimes owing to advances in laser development. The extension of these applications towards the extreme-ultraviolet (EUV) or even x-ray regime has the potential to uncover rich structural and dynamical information with even higher time resolution [17]. However, the technical difficulties with generating EUV or x-ray light sources that achieve both high intensity and temporal coherence hinders such direct applications. Recently, experimental evidence for a time-resolved FWM signal in the EUV regime has been reported using free-electron laser (FEL) pulses with pulse durations of tens of femtoseconds, revealing the dynamics of collective vibrational modes in SiO_2 [16]. However, tracking faster dynamics such as electronic motions requires shorter EUV pulses with a few femtosecond or even subfemtosecond duration. This can be accomplished using high order harmonics (HH), which have have two key characteristics: a broad spectral range spanning from the vacuum-ultraviolet (VUV) to the soft x-ray and regular spectral phase that supports extremely short light burst generation [18,19]. Therefore, HH serve as an excellent FWM mixing source with both wide wavelength tunability and unprecedented time resolution for triggering ultrafast dynamics.

In this Rapid Communication, we report experimental evidence for FWM in the EUV using a HH-based attosecond pulse train (APT). The APT alone cannot induce a nonlinear response in a medium due to its low photon flux. In order to ease the intensity requirement, a strong NIR pulse provides the intensity necessary to achieve an appreciable third-order nonlinear effect. We utilize an APT consisting of three harmonics [11th, 13th (suppressed), and 15th] with an intensity ratio of 40:1:6 to achieve FWM in a neon gas medium. Such a HH pulse contains predominantly a single harmonic (11th harmonic) below the ionization threshold of the neon atom, thus effectively inducing a clean FWM signal that dominates over the background signal at the energy of the 13th harmonic. Figure 1 shows the energy diagram for the FWM process. Ne atoms are resonantly excited to the $3s$ manifold by the APT by absorbing a single photon ω_1 (near 17 eV). The NIR pulse then couples the $3s$ states to the ns/nd manifold near 20 eV by two NIR photons. Since a dark state ($3p$) near resonance with the $3s$ states exists, the two IR photons can be absorbed resonantly, which greatly enhances the third-order nonlinear susceptibility $\chi^{(3)}$. The coherence between the ns/nd states and the ground state forms an oscillating dipole, which emits a photon ω_4 to complete the nonlinear process. As a result of the nonlinear interaction, narrow-band new frequencies in the EUV region with low divergence are observed. The photon flux at these new frequencies grows monotonically with the gas pressure, demonstrating phase matching [10,20]. In addition, the intensities of the newly generated frequency components show a sensitive dynamical dependence on the relative delay between the HH and NIR pulses, in which the information for an electronic wave packet (coherent superposition) is encoded.

II. EXPERIMENTAL METHOD

The experimental setup is similar to an attosecond transient absorption (ATA) configuration [21] as shown in Fig. 1. HH are generated from xenon gas using a 6-fs, 300-μJ few-cycle NIR pulse with a spectrum spanning from 550 to 950 nm. The

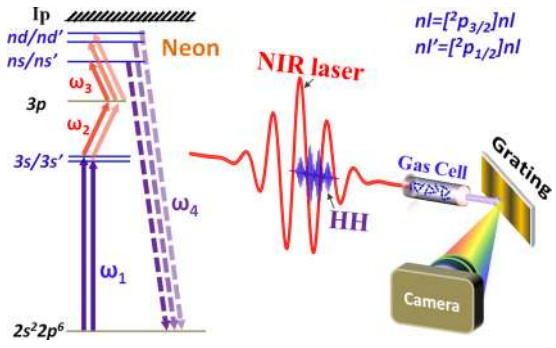

FIG. 1. Energy diagram of the FWM driven by a weak APT and a moderately intense NIR laser.

generated HH pass through a 100-nm indium filter to block the residual NIR field from the HH generating field; an added benefit of the indium filter is dramatic suppression of the 13th harmonic. The harmonics consisting of the dominant 11th and 15th harmonics form an APT with a period of $T_0/4$, which is determined by the energy separation of the two dominant harmonics [18,19]. T_0 is the cycle of the NIR laser. A replica of the few-cycle NIR pulse is picked off from the original pulse and combined spatiotemporally with the APT with an annular mirror. Both the HH and NIR pulses propagate collinearly and are focused into the 1-mm FWM gas cell filled with neon atoms at 0.5–16 Torr. The intensity of the NIR pulse inside the neon gas cell is approximately 2×10^{12} W/cm^2 throughout, except for the intensity-dependent measurement, as shown in Fig. 3(b). The NIR field after the neon FWM gas cell is blocked by a 200-nm aluminum filter. The optical spectrum in the EUV region after the gas cell is recorded by an EUV spectrometer consisting of a flat-field grating and a CCD camera.

III. RESULTS AND DISCUSSION

A. Coherent EUV light generation

The EUV spectrum with and without the neon medium present is shown in Fig. 2. The original HH spectrum consists of three harmonics with the 13th harmonic strongly suppressed by the indium filter, as noted above (see the inset in Fig. 2). The peak intensity ratio of the three harmonics, after correcting for the aluminum filter transmission curve and the CCD camera quantum efficiency, is 40:1:6. Thus the original HH spectrum below the ionization threshold (21.56 eV) of neon is dominated by the 11th harmonic (16.5 eV), which is essential to launch a clean FWM process. When the NIR pulse is switched on during and after the HH attosecond pulses, narrow-bandwidth frequency components with low divergence (see the inset of Fig. 2) in the vicinity of the neon atomic transitions are generated. The widths of the individual emission peaks are limited by the spectrometer resolution (35 meV at 20 eV). These newly generated coherent emissions have a photon energy roughly 3.5 eV above the dominant 11th harmonic (∼16.5 eV), indicating a nonlinear process. A near-resonant FWM process involving a VUV photon (16.8 eV) and two NIR photons (∼1.6 eV) is responsible for the narrow-band EUV light generation based on energy conservation.

The yield of the newly generated EUV components via FWM as a function of gas pressure is shown in Fig. 3(a).

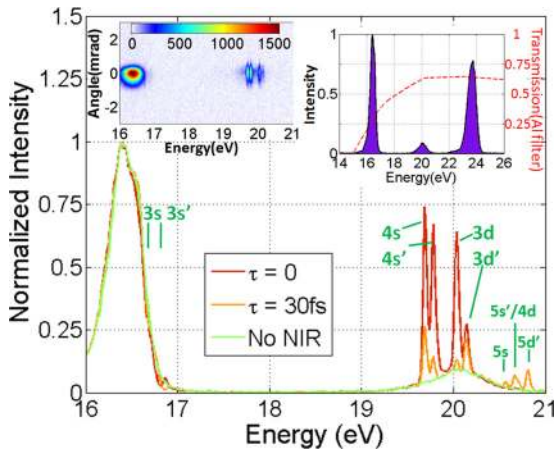

FIG. 2. EUV spectra after the nonlinear medium. The gas pressure is 2.85 Torr. New frequencies are generated when the NIR pulse arrives during (red) and after (orange) the HH pulses. The left inset shows the two-dimensional spectrum on the CCD camera. The right inset is the integrated spectrum without the gas medium. The red dashed line is the transmission curve of the aluminum filter. Spectra are normalized to the peak of the 11th harmonic.

The gas pressure is estimated based on the absorption of the 15th harmonic using the literature absorption cross section of neon above the ionization threshold [22]. The experiment demonstrates a monotonic growth of the EUV emission yield with gas pressure up to 16 Torr (2133 Pa), indicating that phase matching is occurring for efficient EUV source generation. The FWM efficiency can be estimated by dividing the integrated photon flux of the emission features by that of the 11th harmonic; it is approximately 22% at zero delay with a pressure of 16 Torr and quickly drops to a few percent at delays beyond the overlap region. The higher efficiency at zero delay implies an important contribution from nonresonant processes.

The intensity of the emitted feature around 20 eV is determined by two factors: the third-order susceptibility of the corresponding FWM process $\chi^{(3)}$, which describes the nonlinear efficiency per atom, and the phase mismatch between the driving sources and the emitted light, $\Delta\mathbf{k} = \mathbf{k}_{11\text{th}} + \mathbf{k}_{\text{ir1}} + \mathbf{k}_{\text{ir2}} - \mathbf{k}_{\text{euv}}$, which quantifies the coherent buildup of the photon flux through the medium. $\mathbf{k}_{11\text{th}}, \mathbf{k}_{\text{ir1}}, \mathbf{k}_{\text{ir2}}$, and $\mathbf{k}_{\text{euv}}$ represent the wave vectors of the 11th harmonic photon, the two NIR photons, and the generated EUV photon, respectively. In

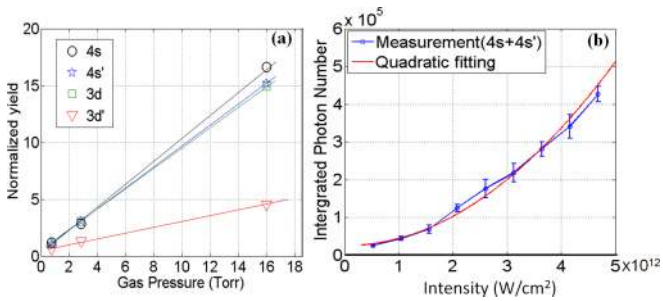

FIG. 3. (a) Integrated intensity of different emission peaks vs the gas pressure. The yield is normalized to the peak of the 11th harmonic. (b) Integrated intensity of the $4s/4s'$ emission features as a function of the NIR intensity. The HH-NIR delay is zero.

the experiment, a loose focusing geometry is used, and the confocal length of both the HH and IR beams is much longer than the length of the gas cell. Therefore, the NIR Gouy phase [23] induced phase mismatch is neglected. The wave vector $\mathbf{k}(\omega)$ is related to the linear susceptibility $\chi^{(1)}(\omega)$ as $\mathbf{k}(\omega) \propto \omega \mathrm{Re}[\sqrt{1+\chi^{(1)}(\omega)}]$, $\chi^{(1)}(\omega) \propto \sum_f \frac{\omega_{gf}\mu_{gf}^2}{\omega_{gf}^2-\omega^2}$. Re denotes the real part, ω_{gf} is the energy difference between the ground state $|g\rangle$ and an excited state $|f\rangle$, and μ_{gf} is the corresponding dipole matrix element. A Taylor expansion of the wave vector to first order gives $\mathbf{k}(\omega) \propto \omega[1+\frac{1}{2}\mathrm{Re}[\chi^{(1)}(\omega)]+\cdots]$, and the phase mismatch reduces to

$$\Delta\mathbf{k} \propto \mathrm{Re}[\omega_{11\mathrm{th}}\chi^{(1)}(\omega_{11\mathrm{th}}) + \omega_{\mathrm{ir1}}\chi^{(1)}(\omega_{\mathrm{ir1}}) + \omega_{\mathrm{ir2}}\chi^{(1)}(\omega_{\mathrm{ir2}}) - \omega_{\mathrm{euv}}\chi^{(1)}(\omega_{\mathrm{euv}})]. \quad (1)$$

The contribution from the far-off-resonance NIR beam to phase mismatch is negligible, therefore $\Delta\mathbf{k}$ is dominated by the two resonant beams, $\omega_{11\mathrm{th}}$ and ω_{euv} [3,9]:

$$\Delta\mathbf{k} \propto \sum_f \omega_{gf}\mu_{gf}^2\left(\frac{\omega_{11\mathrm{th}}}{\omega_{gf}^2-\omega_{11\mathrm{th}}^2} - \frac{\omega_{\mathrm{euv}}}{\omega_{gf}^2-\omega_{\mathrm{euv}}^2}\right). \quad (2)$$

Due to the unmatched frequencies and dipole matrix elements in the two resonant terms of Eq. (2), both transitions need to be red (blue) detuned from the resonance to satisfy the phase matching, therefore greatly reducing the reabsorption of the generated EUV signal. Under the phase-matching condition, the different slopes in Fig. 3(a) indicate different nonlinear susceptibilities $\chi^{(3)}$, for different final states. The maximal gas pressure is limited by the vacuum environment required by the CCD camera, so we expect a brighter EUV source to be generated by increasing the cell length or pressure if the experimental conditions allow.

B. Time-resolved four-wave mixing

The above discussion demonstrates nonlinear generation of narrow-band EUV light using a weak HH field as the mixing source. The HH field is localized in a series of attosecond bursts in the time domain. This allows a time-resolved FWM study to explore the dynamics of a coherent superposition of electronic states initiated by the HH pulses. Figure 4(a) shows the EUV spectra after the neon gas medium as a function of HH-NIR time delay. The onset of narrow-band EUV emissions occurs when the NIR pulse arrives during or immediately after the HH pulse. However, the intensity of each individual emission feature oscillates out to longer times versus time delay. A Fourier analysis of the oscillations [Fig. 4(b)] shows that all the emission features share a common oscillation period of about 25 fs (angular frequency is 0.16 eV/$\hbar$). In addition, the emission features in the vicinity of the $[^2P_{3/2}]4s/[^2P_{1/2}]4s$ to ground-state ($2s^22p^6$) transitions ($\sim$19.75 eV) show a relatively weaker subcycle modulation with a period close to 1.3 fs (angular frequency is 3 eV/$\hbar$).

To understand the various time scales in Fig. 4, we write the polarization induced by the HH and NIR pulse at frequency ω as a power series:

$$\mathbf{p}(\omega) = \varepsilon_0\chi^{(1)}\mathbf{E}_{\mathrm{HH}}(\omega) + \varepsilon_0\chi^{(2)}\mathbf{E}_{\mathrm{HH}}\mathbf{E}_{\mathrm{NIR}} + \varepsilon_0\chi^{(3)}\mathbf{E}_{\mathrm{HH}}\mathbf{E}_{\mathrm{NIR}}\mathbf{E}_{\mathrm{NIR}}. \quad (3)$$

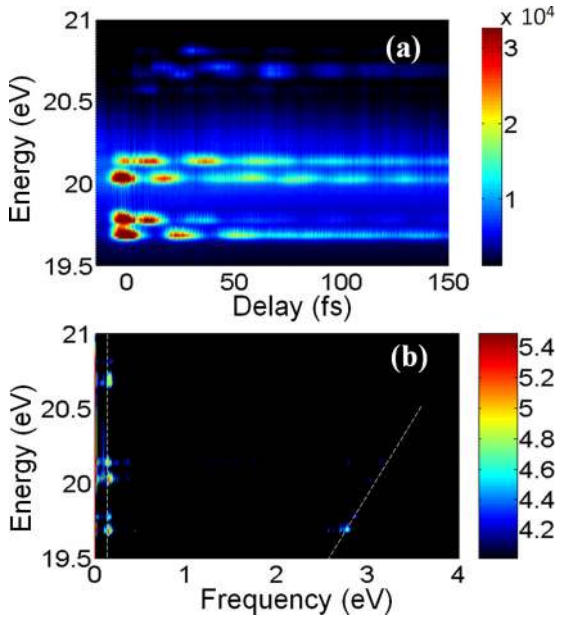

FIG. 4. (a) EUV spectrum as a function of HH-NIR delay: HH attosecond pulses precede the NIR for positive delays. (b) Fourier analysis (logarithm) of the spectrogram in (a) with respect to the delay axis. The gas pressure is 2.85 Torr.

This perturbative treatment is validated by the observed quadratic increase of the FWM yield with the NIR intensity as shown in Fig. 3(b). The first term in Eq. (3) is the linear response of neon gas to the HH field. The second term typically vanishes due to the inversion symmetry of the atomic system. The third term represents the nonlinear FWM process discussed in this work. For a broadband HH driving source that can provide frequencies to drive both the first (one-photon pathway) and the third term (three-photon pathway), modulations in the intensity of absorption lines are expected due to the interference of the two pathways. This is the characteristic of a typical ATA experiment, and the "which-way" interference is the main mechanism of various oscillation features. As a result, the oscillation frequencies of different absorption lines lie on a line oriented at 45° [24–29]. We therefore attribute the very fast oscillations with frequencies around 3 eV/$\hbar$; (period of 1.3 fs) lying on a 45° line in Fig. 4(b) to the one-photon versus three-photon pathway interference. In this experiment, the 13th harmonic that drives the first-order process is strongly suppressed, and the spectrum near 20 eV is predominantly contributed by the third-order nonlinearity, resulting in a rather weak subcycle oscillation related to the "which-way" interference.

Two spin-orbit split states, $[^2P_{3/2}]3s$ and $[^2P_{1/2}]3s$, are simultaneously populated by the 11th harmonic, and two three-photon pathways can reach the same final state around 20 eV and also interfere; this is the dominant interference mechanism in the current FWM experiment. A time-resolved study can directly map out the beating frequency between the two states that are formed in a coherent superposition by the HH driving pulse. Therefore, we attribute the slow frequency components lying on a vertical line in Fig. 4(b) to quantum beating between the $[^2P_{3/2}]3s$ and $[^2P_{1/2}]3s$ electronic states (splitting approximately 0.17 eV). Note that the oscillations

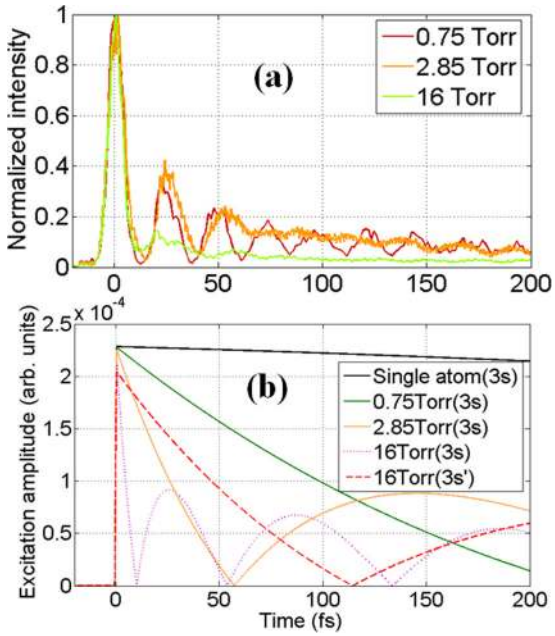

FIG. 5. (a) Measured delay-dependent yield of the 4s emission feature under different gas pressures. (b) Calculated excitation amplitudes of $3s/3s'$ states by the HH pulse; the interaction length is 1 mm. Dipole matrix elements are adapted from Ref. [22].

of the EUV emission features show different phases. This indicates the competition between different FWM channels that share the transferred population from the same initial $3s/3s'$ states.

The results presented here differ from a recent study of neon using ATA spectroscopy that reported wave-packet dynamics imprinted on the absorption spectrum at similar photon energies [27]. That work revealed a longer modulation period (45 fs), corresponding to the energy spacing between two NIR coupled bright states ($[^2P_{1/2}]3d$ and $[^2P_{3/2}]3d$) and arising from interference between the first- and third-order terms in Eq. (3). Previous studies using photoelectron spectroscopy successfully observed both quantum beats and "which-way" interference of helium atoms with scattering states as the final states [30]. Here, we demonstrate an all-optical method of FWM with a bound state as the final state for detecting both types of ultrafast dynamic information of a bound electronic wave packet.

In the measurement shown in Fig. 4, the emission intensity decays quickly as the delay increases. The line-out at the energy corresponding to the 4s emission feature versus delay is shown in Fig. 5(a) for different gas pressures. As the pressure increases, the decay becomes more severe and the quantum beat information is gradually lost. This indicates that macroscopic propagation effects are playing a significant role in the resulting spectrogram. The temporal structure of the HH pulse train at the beginning of the gas medium is a regular APT with a duration of a few femtoseconds. Thus the excitation is prompt and serves as a precise timing tool to start the nonlinear process. As the HH pulse propagates through the resonant medium, its temporal structure will be elongated and distorted due to the interplay between the induced polarization and the original pulse [31–33]. Consequently, the initial excitation by the HH pulse is no longer prompt but persists for a longer time, thereby losing the ability to precisely clock the nonlinear process.

To get a better glimpse of the physical picture, we use a two-level model coupled with the one-dimensional (1D) Maxwell's equation to simulate the interaction of an APT with a neon gas medium; only the ground state and one of the excited states ($[^2P_{3/2}]3s$ or $[^2P_{1/2}]3s$) are considered. The calculated results are shown in Fig. 5(b). The population amplitude of the excited state decays quickly as the medium pressure is increased. Thus the effective nonlinear susceptibility $\chi^{(3)}$ is reduced by the loss of coherence as the NIR pulse is introduced at later times, explaining the decay observed in the experiment. Since the dipole matrix elements related to the $[^2P_{3/2}]3s$ and $[^2P_{1/2}]3s$ differ by a factor of three, as the propagation effects become important, their excitation amplitudes show rather different time structures, as shown in Fig. 5(b). This difference is imprinted on the measurement shown in Fig. 5(a) and blurs the quantum beating signal between the $[^2P_{3/2}]3s$ and $[^2P_{1/2}]3s$ states. The experimentally observed faster decay around zero delay is related to the nonresonant contribution that is ignored in the model calculation [34,35]. Although the bright EUV emissions in the vicinity of the transitions prefer higher gas pressure due to preserved phase matching, the retrieval of accurate dynamical information requires a lower gas pressure where the distortion of the resonant excitation pulse is not too severe to degrade its timing ability. This differentiates the two conditions needed for the two applications of the current experimental method.

IV. CONCLUSION

In conclusion, we experimentally demonstrated the nonlinear response of neon gas to an APT synchronized with a NIR laser pulse. New frequency components in the EUV region, featuring narrow bandwidth and low divergence, are generated by a near-resonant four-wave mixing process. The efficiency of the nonlinear emission intensity grows monotonically with gas pressure, revealing the phase-matching nature of the phenomenon. A time-resolved study of this nonlinear interaction successfully recovers the recurrence of bound-state electronic wave-packet motion initiated by the attosecond pulses by FWM detection in the EUV. This homodyne detection method not only provides an efficient route for coherent EUV source generation, but also offers a background-free nonlinear EUV signal for accessing clean dynamics following electronic excitation, which is generally challenging in ATA spectroscopy due to the complex mixture of multiple physical processes. This all-optical methodology holds promise to be extended to more complex systems, such as molecules, for applications including tunable bright coherent light generation and time-resolved ultrafast dynamics driven by electronic-nuclear coupling.

ACKNOWLEDGMENT

This work was supported by the Director, Office of Science, Office of Basic Energy Sciences, and by the Division of Chemical Sciences, Geosciences, and Biosciences of the U.S. Department of Energy at LBNL under Contract No. DE-AC02-05CH11231.

[1] S. Mukamel, *Principles of Nonlinear Optical Spectroscopy* (Oxford University Press, Oxford, U.K., 1999).
[2] P. Hamm and M. Zanni, *Concepts and Methods of 2D Infrared Spectroscopy* (Cambridge University Press, Cambridge, U.K., 2011).
[3] R. Mahon, T. J. McIlrath, V. P. Myerscough, and D. W. Koopman, IEEE J. Quantum Electron. **15**, 444 (1979).
[4] R. Wallenstein, Opt. Commun. **33**, 119 (1980).
[5] K. S. E. Eikema, J. Walz, and T. W. Hänsch, Phys. Rev. Lett. **83**, 3828 (1999).
[6] L. Misoguti, I. P. Christov, S. Backus, M. M. Murnane, and H. C. Kapteyn, Phys. Rev. A **72**, 063803 (2005).
[7] J. B. Bertrand, H. J. Wörner, H. C. Bandulet, E. Bisson, M. Spanner, J. C. Kieffer, D. M. Villeneuve, and P. B. Corkum, Phys. Rev. Lett. **106**, 023001 (2011).
[8] T. E. Glover *et al.*, Nature (London) **488**, 603 (2012).
[9] D. Kolbe, M. Scheid, and J. Walz, Phys. Rev. Lett. **109**, 063901 (2012).
[10] M. Chini *et al.*, Nat. Photonics **8**, 437 (2014).
[11] P. Tzallas, E. Skantzakis, L. A. A. Nikolopoulos, G. D. Tsakiris, and D. Charalambidis, Nat. Phys. **7**, 781 (2011).
[12] T. K. Allison, T. W. Wright, A. M. Stooke, C. Khurmi, J. V. Tilborg, Y. Liu, R. W. Falcone, and A. Belkacem, Opt. Lett. **35**, 3664 (2010).
[13] Y. Furukawa, Y. Nabekawa, T. Okino, S. Saugout, K. Yamanouchi, and K. Midorikawa, Phys. Rev. A **82**, 013421 (2010).
[14] W. Cao, G. Laurent, I. Ben-Itzhak, and C. L. Cocke, Phys. Rev. Lett. **114**, 113001 (2015).
[15] M. Schultze *et al.*, Science **346**, 1348 (2014).
[16] F. Bencivenga *et al.*, Nature (London) **520**, 205 (2015).
[17] I. V. Schweigert and S. Mukamel, Phys. Rev. Lett. **99**, 163001 (2007).
[18] P. Antoine, A. L'Huillier, and M. Lewenstein, Phys. Rev. Lett. **77**, 1234 (1996).
[19] P. M. Paul, E. S. Toma, P. Breger, Genevive Mullot, F. Augé, Ph. Balcou, H. G. Muller, and P. Agostini, Science **292**, 1689 (2001).
[20] E. Constant, D. Garzella, P. Breger, E. Mével, Ch. Dorrer, C. Le Blanc, F. Salin, and P. Agostini, Phys. Rev. Lett. **82**, 1668 (1999).
[21] A. R. Beck, D. M. Neumark, and S. R. Leone, Chem. Phys. Lett. **624**, 119 (2015).
[22] W. F. Chan, G. Cooper, X. Guo, and C. E. Brion, Phys. Rev. A **45**, 1420 (1992).
[23] F. Lindner, G. G. Paulus, H. Walther, A. Baltuška, E. Goulielmakis, M. Lezius, and F. Krausz, Phys. Rev. Lett. **92**, 113001 (2004).
[24] M. Chini, X. Wang, Y. Cheng, Y. Wu, D. Zhao, D. A. Telnov, S.-I. Chu, and Z. Chang, Sci. Rep. **3**, 1105 (2013).
[25] S. Chen, M. Wu, M. B. Gaarde, and K. J. Schafer, Phys. Rev. A **87**, 033408 (2013).
[26] A. Blättermann, C. Ott, A. Kaldun, T. Ding, and T. Pfeifer, J. Phys. B **47**, 124008 (2014).
[27] A. R. Beck, B. Bernhardt, E. R. Warrick, M. Wu, S. Chen, M. B. Gaarde, K. J. Schafer, D. M. Neumark, and S. R. Leone, New J. Phys. **16**, 113016 (2014).
[28] W. Cao, E. R. Warrick, D. M. Neumark, and S. R. Leone, New J. Phys. **18**, 013041 (2016).
[29] T. Ding *et al.*, Opt. Lett. **41**, 709 (2016).
[30] J. Mauritsson, T. Remetter, M. Swoboda, K. Klunder, A. L'Huillier, K. J. Schafer, O. Ghafur, F. Kelkensberg, W. Siu, P. Johnsson, M. J. J. Vrakking, I. Znakovskaya, T. Uphues, S. Zherebtsov, M. F. Kling, F. Lepine, E. Benedetti, F. Ferrari, G. Sansone, and M. Nisoli, Phys. Rev. Lett. **105**, 053001 (2010).
[31] M. D. Crisp, Phys. Rev. A **1**, 1604 (1970).
[32] M. B. Gaarde, C. Buth, J. L. Tate, and K. J. Schafer, Phys. Rev. A **83**, 013419 (2011).
[33] C. T. Liao, A. Sandhu, S. Camp, K. J. Schafer, and M. B. Gaarde, Phys. Rev. Lett. **114**, 143002 (2015).
[34] W. Zinth, A. Laubereau, and W. Kaiser, Opt. Commun. **26**, 457 (1978).
[35] R. Leonhardt, W. Holzapfel, W. Zinth, and W. Kaiser, Chem. Phys. Lett. **133**, 373 (1987).